

Calculating photonic Green's functions using a non-orthogonal finite difference time domain method

A. J. Ward, J. B. Pendry

Condensed Matter Theory Group, The Blackett Laboratory, Imperial College, London, SW7 2BZ, UK
(December 31, 2021)

In this paper we shall propose a simple scheme for calculating Green's functions for photons propagating in complex structured dielectrics or other photonic systems. The method is based on an extension of the finite difference time domain (FDTD) method, originally proposed by Yee¹, also known as the Order-N method², which has recently become a popular way of calculating photonic band structures. We give a new, transparent derivation of the Order-N method which, in turn, enables us to give a simple yet rigorous derivation of the criterion for numerical stability as well as statements of charge and energy conservation which are exact even on the discrete lattice. We implement this using a general, non-orthogonal co-ordinate system without incurring the computational overheads normally associated with non-orthogonal FDTD.

We present results for local densities of states calculated using this method for a number of systems. Firstly, we consider a simple one dimensional dielectric multilayer, identifying the suppression in the state density caused by the photonic band gap and then observing the effect of introducing a defect layer into the periodic structure. Secondly, we tackle a more realistic example by treating a defect in a crystal of dielectric spheres on a diamond lattice. This could have application to the design of super-efficient laser devices utilising defects in photonic crystals as laser cavities.

PACS numbers: 42.70.Qs, 02.70.Bf, 02.70.-c

I. INTRODUCTION

One of the principle driving forces behind the recent flurry of research into photonic band gap materials^{3,4} has been the potential for manipulating the spontaneous emission of an atom placed in a cavity in such a material. As was pointed out some years ago⁵ a material with a periodically structured dielectric function (a photonic crystal) can have a profound effect on the density of states for photons within the material, in some cases leading to frequency windows for which no allowed photon states exist. These windows, or photonic band gaps, radically alter the emission properties of atoms. An excited atom that wants to emit a photon of a frequency within the band gap cannot do so—the photon has no states into which it can go and so is forced to form a new kind of atom-photon bound state. Even zero-point fluctuations are forbidden within the band gap. This has immediate implications for device physics. Placing an active device, such as a semiconductor laser, within a cavity in a photonic crystal offers the possibility to control unwanted spontaneous emission and allow emission only into the lasing mode, thus dramatically improving the efficiency of the device⁶.

Green's functions have the potential to play a central role in the theoretical investigations of these photonic systems. Not only are they a natural way to express key quantities such as the density of states, they are also easily calculated within the framework of time domain methods such as the Order N technique that we shall be exploring in this paper. In systems where dissipation is present, such as those containing metals or lossy dielectrics, the Green's function approach is the only route to calculate quantities of physical interest.

For the theorist, the challenge is to solve Maxwell's equations for such systems. Much progress has been made in the past few years and several well established techniques have emerged. Probably the most widely used is the Plane Wave method⁷⁻⁹. Simply put, this method involves expanding the electromagnetic fields as a sum of plane waves and recasting Maxwell's equations into the form of an eigenvalue problem to find the allowed eigenfrequencies. Though simple to implement and use, this method has the draw back that the time taken for the calculation scales as the cube of the number of plane waves used, so for complicated problems which require many plane waves this is a severe limitation. Another limitation is to systems whose dielectric functions do not disperse with frequency. Hence metallic systems are beyond the scope of this method.

A second popular method involves working at a fixed frequency but instead of expanding the wavefield on a lattice in reciprocal space the wavefield is represented on the points of a real space lattice^{10,11}. The resulting equations can be rearranged into the form of a Transfer Matrix which relates the fields in one layer of the lattice to the fields in the next. This method has proved extremely useful especially for systems involving metals where the dielectric constant is a function of frequency. Also, because the form the transfer matrix takes, connecting the fields on one *surface* to

the fields on another, calculations based on this method scale as the square of the number of real space points, rather than the cube.

This may be an improvement over the plane wave method but is still worse than the optimal linear scaling with system size. However, it has been shown² that, because Maxwell's equations are local then by working in the time domain instead of the frequency domain it is possible to obtain methods which scale as 'order N ' where N is the system size. We shall work with such a method in this paper in order to calculate photonic Green's functions and from those other quantities of physical interest such as densities of states. Previous work has successfully calculated spontaneous emission rates from the density of states using a real space lattice formulation¹². However, that work was based in the frequency domain. By working in the time domain we are able to exploit the more favourable scaling law and consider larger, more complex systems such as photonic crystals with defects.

II. METHODS

The theory behind the methods used in this paper is somewhat similar in principle to the Finite Difference Time Domain method first introduced to the electrical engineering community by Yee¹ in 1966, and first applied to the problem of photonic band structures by Chan *et al.*² in 1995. Here we present a systematic derivation of the finite difference equations within a transparent formalism. The advantages of this new formalism over the traditional Yee approach are many. First, it makes clear how to find quantities which are exactly conserved even by the discrete equations. Hence we can identify the analogies to charge, energy density and the Poynting vector *etc.* Second, our formalism enables the precise analysis of the stability of the discrete equations to be made from a simple consideration of the approximations involved, sidestepping the usual, rather involved, Courant stability analysis. Third, and perhaps most importantly, the new formalism shows, for the first time, how to present the finite difference equations in a completely general co-ordinate system without incurring the computational overheads normally associated with non-orthogonal FDTD¹³. Finally, it is hoped that this transparency will make it simpler to extend the method to areas to which it has not yet been applied. We begin from the usual Maxwell's equations, neglecting any free charges or currents;

$$\nabla \times \mathbf{H} = \varepsilon_0 \varepsilon(\mathbf{r}) \frac{\partial \mathbf{E}}{\partial t} \quad \nabla \times \mathbf{E} = -\mu_0 \mu(\mathbf{r}) \frac{\partial \mathbf{H}}{\partial t} \quad (1)$$

which on Fourier transforming into (\mathbf{K}, ω) space can be written,

$$i\mathbf{k} \times \mathbf{H} = -i\varepsilon_0 \varepsilon \omega \mathbf{E} \quad i\mathbf{k} \times \mathbf{E} = +i\mu_0 \mu \omega \mathbf{H} \quad (2)$$

Next we wish to place these equations onto a discrete, real space lattice by replacing the derivatives with finite differences. We have some freedom here but must be careful—not all differencing schemes lead to stable equations. We will take our lead therefore from the differencing scheme which has proved so successful in the transfer matrix method¹¹. We do this by introducing the following approximations to ω and \mathbf{k} . For the terms which involve the electric field we use,

$$k_x \mapsto k_x^+ = \frac{e^{ik_x a} - 1}{ia} \quad \omega \mapsto \omega^+ = \frac{e^{(-i\omega\delta t)} - 1}{-i\delta t} \quad (3)$$

with similar expressions for k_y^+ and k_z^+ . For the magnetic field terms we use,

$$k_x \mapsto k_x^- = \frac{1 - e^{(-ik_x a)}}{ia} \quad \omega \mapsto \omega^- = \frac{1 - e^{(i\omega\delta t)}}{-i\delta t} \quad (4)$$

etc. So making these approximations in equation (2) we get,

$$i\mathbf{k}^- \times \mathbf{H} = -i\varepsilon_0 \varepsilon \omega^+ \mathbf{E} \quad i\mathbf{k}^+ \times \mathbf{E} = +i\mu_0 \mu \omega^- \mathbf{H} \quad (5)$$

On Fourier transforming back into the (\mathbf{r}, t) domain it is clear that these approximations are equivalent to taking a forward finite difference, Δ^+ , in place of derivatives of the electric field, and a backwards difference, Δ^- , for derivatives of the magnetic field.

$$\Delta_x^+ \mathcal{F}(\mathbf{r}) = [\mathcal{F}(\mathbf{r} + \mathbf{a}) - \mathcal{F}(\mathbf{r})] / a \quad (6)$$

$$\Delta_x^- \mathcal{F}(\mathbf{r}) = [\mathcal{F}(\mathbf{r}) - \mathcal{F}(\mathbf{r} - \mathbf{a})] / a \quad (7)$$

Putting it all together the discrete form of Maxwell's equations become,

$$\nabla^+ \times \mathbf{E}(\mathbf{r}, t) = -\mu_0 \hat{\mu}(\mathbf{r}) \Delta_t^- \mathbf{H}(\mathbf{r}, t) \quad (8)$$

$$\nabla^- \times \mathbf{H}(\mathbf{r}, t) = \varepsilon_0 \hat{\varepsilon}(\mathbf{r}) \Delta_t^+ \mathbf{E}(\mathbf{r}, t) \quad (9)$$

where,

$$\nabla^+ \times = \begin{pmatrix} 0 & -\Delta_z^+ & \Delta_y^+ \\ \Delta_z^+ & 0 & -\Delta_x^+ \\ -\Delta_y^+ & \Delta_x^+ & 0 \end{pmatrix} \quad (10)$$

$$\nabla^- \times = \begin{pmatrix} 0 & -\Delta_z^- & \Delta_y^- \\ \Delta_z^- & 0 & -\Delta_x^- \\ -\Delta_y^- & \Delta_x^- & 0 \end{pmatrix} \quad (11)$$

The approximations outlined in the previous paragraph place Maxwell's equations onto a discrete lattice of points which is uniform and Cartesian. However, this is not always convenient for the problems we may want to consider. It may be to our advantage to work in a co-ordinate system which is non-uniform or even non-orthogonal. Fortunately, as shown in detail elsewhere¹⁴ there is a simple result which allows us to map a completely arbitrary co-ordinate system onto a uniform Cartesian one as long as we introduce new, renormalised versions of the permittivity and permeability. In the generalised co-ordinates Maxwell's equations become,

$$\frac{\nabla_q^- \times \hat{\mathbf{H}}(\mathbf{r}, t)}{Q_0} = \varepsilon_0 \hat{\varepsilon}(\mathbf{r}) \frac{\Delta_\tau^+ \hat{\mathbf{E}}(\mathbf{r}, t)}{\delta t} \quad (12)$$

$$\frac{\nabla_q^+ \times \hat{\mathbf{E}}(\mathbf{r}, t)}{Q_0} = -\mu_0 \hat{\mu}(\mathbf{r}) \frac{\Delta_\tau^- \hat{\mathbf{H}}(\mathbf{r}, t)}{\delta t} \quad (13)$$

where,

$$\Delta_{q_1}^+ \mathcal{F}(\mathbf{r}, t) = \mathcal{F}(\mathbf{r} + Q_1 \mathbf{u}_1, t) - \mathcal{F}(\mathbf{r}, t) \quad \Delta_\tau^+ \mathcal{F}(\mathbf{r}, t) = \mathcal{F}(\mathbf{r}, t + \delta t) - \mathcal{F}(\mathbf{r}, t) \quad (14)$$

$$\Delta_{q_1}^- \mathcal{F}(\mathbf{r}, t) = \mathcal{F}(\mathbf{r}, t) - \mathcal{F}(\mathbf{r} - Q_1 \mathbf{u}_1, t) \quad \Delta_\tau^- \mathcal{F}(\mathbf{r}, t) = \mathcal{F}(\mathbf{r}, t) - \mathcal{F}(\mathbf{r}, t - \delta t) \quad (15)$$

etc,

$$\hat{\varepsilon}^{ij}(\mathbf{r}) = \varepsilon(\mathbf{r}) g^{ij} |\mathbf{u}_1 \cdot \mathbf{u}_2 \times \mathbf{u}_3| \frac{Q_1 Q_2 Q_3}{Q_i Q_j Q_0} \quad \hat{\mu}^{ij}(\mathbf{r}) = \mu(\mathbf{r}) g^{ij} |\mathbf{u}_1 \cdot \mathbf{u}_2 \times \mathbf{u}_3| \frac{Q_1 Q_2 Q_3}{Q_i Q_j Q_0} \quad (16)$$

and

$$\hat{\sigma}^{ij}(\mathbf{r}) = \sigma(\mathbf{r}) g^{ij} |\mathbf{u}_1 \cdot \mathbf{u}_2 \times \mathbf{u}_3| \frac{Q_1 Q_2 Q_3}{Q_i Q_j Q_0} \quad \hat{\sigma}_m^{ij}(\mathbf{r}) = \sigma_m(\mathbf{r}) g^{ij} |\mathbf{u}_1 \cdot \mathbf{u}_2 \times \mathbf{u}_3| \frac{Q_1 Q_2 Q_3}{Q_i Q_j Q_0} \quad (17)$$

The generalised co-ordinate system is defined by the three unit vectors, \mathbf{u}_1 , \mathbf{u}_2 and \mathbf{u}_3 which point along the generalised co-ordinate axis and the three lattice spacings Q_1 , Q_2 and Q_3 which define the spacing between discrete lattice points in each direction. In general, the \mathbf{u}_i 's and Q_i 's will themselves be functions of position. The metric tensor g^{ij} is defined such that $(g^{-1})^{ij} = \mathbf{u}_i \cdot \mathbf{u}_j$. As well as the permittivity and permeability being renormalised by the co-ordinate transformation, the fields themselves are also rescaled by the lattice spacings,

$$\hat{E}_i = Q_i E_i \quad \hat{H}_i = Q_i H_i \quad (18)$$

In order to obtain the equations that will link the fields at one time step to the fields at the next we introduce,

$$\hat{\mathbf{H}}' = \frac{\delta t}{\varepsilon_0 Q_0} \hat{\mathbf{H}} \quad (19)$$

and let,

$$\mathbf{a} = Q_1 \mathbf{u}_1 \quad \mathbf{b} = Q_2 \mathbf{u}_2 \quad \mathbf{c} = Q_3 \mathbf{u}_3 \quad (20)$$

Then after some rearranging we arrive at,

$$\begin{aligned} \hat{E}_1(\mathbf{r}, t + \delta t) &= \hat{E}_1(\mathbf{r}, t) + [\hat{\varepsilon}^{-1}(\mathbf{r})]^{11} [\hat{H}'_3(\mathbf{r}, t) - \hat{H}'_3(\mathbf{r} - \mathbf{b}, t) - \hat{H}'_2(\mathbf{r}, t) + \hat{H}'_2(\mathbf{r} - \mathbf{c}, t)] \\ &\quad + [\hat{\varepsilon}^{-1}(\mathbf{r})]^{12} [\hat{H}'_1(\mathbf{r}, t) - \hat{H}'_1(\mathbf{r} - \mathbf{c}, t) - \hat{H}'_3(\mathbf{r}, t) + \hat{H}'_3(\mathbf{r} - \mathbf{a}, t)] \\ &\quad + [\hat{\varepsilon}^{-1}(\mathbf{r})]^{13} [\hat{H}'_2(\mathbf{r}, t) - \hat{H}'_2(\mathbf{r} - \mathbf{a}, t) - \hat{H}'_1(\mathbf{r}, t) + \hat{H}'_1(\mathbf{r} - \mathbf{b}, t)] \end{aligned} \quad (21)$$

$$\begin{aligned} \hat{E}_2(\mathbf{r}, t + \delta t) &= \hat{E}_2(\mathbf{r}, t) + [\hat{\varepsilon}^{-1}(\mathbf{r})]^{21} [\hat{H}'_3(\mathbf{r}, t) - \hat{H}'_3(\mathbf{r} - \mathbf{b}, t) - \hat{H}'_2(\mathbf{r}, t) + \hat{H}'_2(\mathbf{r} - \mathbf{c}, t)] \\ &\quad + [\hat{\varepsilon}^{-1}(\mathbf{r})]^{22} [\hat{H}'_1(\mathbf{r}, t) - \hat{H}'_1(\mathbf{r} - \mathbf{c}, t) - \hat{H}'_3(\mathbf{r}, t) + \hat{H}'_3(\mathbf{r} - \mathbf{a}, t)] \\ &\quad + [\hat{\varepsilon}^{-1}(\mathbf{r})]^{23} [\hat{H}'_2(\mathbf{r}, t) - \hat{H}'_2(\mathbf{r} - \mathbf{a}, t) - \hat{H}'_1(\mathbf{r}, t) + \hat{H}'_1(\mathbf{r} - \mathbf{b}, t)] \end{aligned} \quad (22)$$

$$\begin{aligned} \hat{E}_3(\mathbf{r}, t + \delta t) &= \hat{E}_3(\mathbf{r}, t) + [\hat{\varepsilon}^{-1}(\mathbf{r})]^{31} [\hat{H}'_3(\mathbf{r}, t) - \hat{H}'_3(\mathbf{r} - \mathbf{b}, t) - \hat{H}'_2(\mathbf{r}, t) + \hat{H}'_2(\mathbf{r} - \mathbf{c}, t)] \\ &\quad + [\hat{\varepsilon}^{-1}(\mathbf{r})]^{32} [\hat{H}'_1(\mathbf{r}, t) - \hat{H}'_1(\mathbf{r} - \mathbf{c}, t) - \hat{H}'_3(\mathbf{r}, t) + \hat{H}'_3(\mathbf{r} - \mathbf{a}, t)] \\ &\quad + [\hat{\varepsilon}^{-1}(\mathbf{r})]^{33} [\hat{H}'_2(\mathbf{r}, t) - \hat{H}'_2(\mathbf{r} - \mathbf{a}, t) - \hat{H}'_1(\mathbf{r}, t) + \hat{H}'_1(\mathbf{r} - \mathbf{b}, t)] \end{aligned} \quad (23)$$

$$\begin{aligned} \hat{H}'_1(\mathbf{r}, t + \delta t) &= \hat{H}'_1(\mathbf{r}, t) \\ &\quad - \left(\frac{\delta t c_0}{Q_0} \right)^2 [\hat{\mu}^{-1}(\mathbf{r})]^{11} [\hat{E}_3(\mathbf{r} + \mathbf{b}, t) - \hat{E}_3(\mathbf{r}, t) - \hat{E}_2(\mathbf{r} + \mathbf{c}, t) + \hat{E}_2(\mathbf{r}, t)] \\ &\quad - \left(\frac{\delta t c_0}{Q_0} \right)^2 [\hat{\mu}^{-1}(\mathbf{r})]^{12} [\hat{E}_1(\mathbf{r} + \mathbf{c}, t) - \hat{E}_1(\mathbf{r}, t) - \hat{E}_3(\mathbf{r} + \mathbf{a}, t) + \hat{E}_3(\mathbf{r}, t)] \\ &\quad - \left(\frac{\delta t c_0}{Q_0} \right)^2 [\hat{\mu}^{-1}(\mathbf{r})]^{13} [\hat{E}_2(\mathbf{r} + \mathbf{a}, t) - \hat{E}_2(\mathbf{r}, t) - \hat{E}_1(\mathbf{r} + \mathbf{b}, t) + \hat{E}_1(\mathbf{r}, t)] \end{aligned} \quad (24)$$

$$\begin{aligned} \hat{H}'_2(\mathbf{r}, t + \delta t) &= \hat{H}'_2(\mathbf{r}, t) \\ &\quad - \left(\frac{\delta t c_0}{Q_0} \right)^2 [\hat{\mu}^{-1}(\mathbf{r})]^{21} [\hat{E}_3(\mathbf{r} + \mathbf{b}, t) - \hat{E}_3(\mathbf{r}, t) - \hat{E}_2(\mathbf{r} + \mathbf{c}, t) + \hat{E}_2(\mathbf{r}, t)] \\ &\quad - \left(\frac{\delta t c_0}{Q_0} \right)^2 [\hat{\mu}^{-1}(\mathbf{r})]^{22} [\hat{E}_1(\mathbf{r} + \mathbf{c}, t) - \hat{E}_1(\mathbf{r}, t) - \hat{E}_3(\mathbf{r} + \mathbf{a}, t) + \hat{E}_3(\mathbf{r}, t)] \\ &\quad - \left(\frac{\delta t c_0}{Q_0} \right)^2 [\hat{\mu}^{-1}(\mathbf{r})]^{23} [\hat{E}_2(\mathbf{r} + \mathbf{a}, t) - \hat{E}_2(\mathbf{r}, t) - \hat{E}_1(\mathbf{r} + \mathbf{b}, t) + \hat{E}_1(\mathbf{r}, t)] \end{aligned} \quad (25)$$

$$\begin{aligned} \hat{H}'_3(\mathbf{r}, t + \delta t) &= \hat{H}'_3(\mathbf{r}, t) \\ &\quad - \left(\frac{\delta t c_0}{Q_0} \right)^2 [\hat{\mu}^{-1}(\mathbf{r})]^{31} [\hat{E}_3(\mathbf{r} + \mathbf{b}, t) - \hat{E}_3(\mathbf{r}, t) - \hat{E}_2(\mathbf{r} + \mathbf{c}, t) + \hat{E}_2(\mathbf{r}, t)] \\ &\quad - \left(\frac{\delta t c_0}{Q_0} \right)^2 [\hat{\mu}^{-1}(\mathbf{r})]^{32} [\hat{E}_1(\mathbf{r} + \mathbf{c}, t) - \hat{E}_1(\mathbf{r}, t) - \hat{E}_3(\mathbf{r} + \mathbf{a}, t) + \hat{E}_3(\mathbf{r}, t)] \\ &\quad - \left(\frac{\delta t c_0}{Q_0} \right)^2 [\hat{\mu}^{-1}(\mathbf{r})]^{33} [\hat{E}_2(\mathbf{r} + \mathbf{a}, t) - \hat{E}_2(\mathbf{r}, t) - \hat{E}_1(\mathbf{r} + \mathbf{b}, t) + \hat{E}_1(\mathbf{r}, t)] \end{aligned} \quad (26)$$

These equations allow us to take an arbitrary set of electric and magnetic fields at some initial time $t = 0$ and, subject to appropriate boundary conditions, calculate the fields at all later times.

Notice that by incorporating all of the details of the generalised co-ordinate system into the new definitions of the permittivity and permeability we have, in effect, eliminated the extra computational overhead of the general co-ordinates. If the co-ordinate system changed from one place to another, and there is no reason why it should not, we would have to store the metric tensor at each point on the lattice. But since we have to store ε and μ tensors at each point anyway, by combining the metric into our new $\hat{\varepsilon}$ and $\hat{\mu}$ we cut the amount of storage needed. Similarly, we also reduce the number of calculations required at each time step as we no longer need to worry about converting between covariant and contravariant vectors at every time step - this is all taken care of by $\hat{\varepsilon}$ and $\hat{\mu}$. Hence, in contrast with previous methods, our non-orthogonal FDTD has no additional computational overhead compared to an orthogonal one, except for the initial setting up of $\hat{\varepsilon}$ and $\hat{\mu}$.

A. Stability Criterion

These equations give a stable updating procedure for the fields if the time step is kept sufficiently small. The criterion is easy to find. Starting from the approximations we made for \mathbf{k} and ω , (equations 3 and 4) the free space dispersion relation, $\omega^2 = c_0^2 k^2$, becomes,

$$\frac{4}{\delta t^2} \sin^2 \left(\frac{\omega \delta t}{2} \right) = 4c_0^2 \left[\frac{1}{Q_1^2} \sin^2 \left(\frac{Q_1 k_x}{2} \right) + \frac{1}{Q_2^2} \sin^2 \left(\frac{Q_2 k_y}{2} \right) + \frac{1}{Q_3^2} \sin^2 \left(\frac{Q_3 k_z}{2} \right) \right] \quad (27)$$

The condition that the maximum value of the right hand side must correspond to a real frequency gives,

$$(\delta t)^2 < \left(\frac{c_0^2}{Q_1^2} + \frac{c_0^2}{Q_2^2} + \frac{c_0^2}{Q_3^2} \right)^{-1} \quad (28)$$

B. Fourier Transforms

The final step of any time domain method is a Fourier transform of the time dependent information into the frequency domain, and for our FDTD method there are a few points which need to be made clear. Firstly, it is desirable to eliminate the zero frequency, longitudinal mode from our results. This is done by subtracting off the static part from the time dependent fields which we have calculated so that their time average is zero. Next, we must ensure that we obtain the properly causal solution to Maxwell's equations when we replace the integral in the Fourier transform with a discrete sum. We do this by adding a small positive, imaginary part δ to the frequency.

$$\int_{-\infty}^{\infty} f(t) \exp [i\omega t] dt \mapsto \sum_{n=1}^{N_t} f(n \delta t) \exp [i(\omega + i\delta) (n \pm 1/2)\delta t] \quad (29)$$

The size of this imaginary part is determined by the total time interval over which the fields are integrated. In order to be properly causal, the final term in the sum must tend to zero. This is of less importance when finding a band structure but is critical if we are to calculate the Green's function correctly. Another small detail - because of the choices we have made in our approximations for the time derivatives for \mathbf{E} and \mathbf{H} , it is necessary to include a half time step offset, minus for the \mathbf{E} field and plus for the \mathbf{H} .

C. Conserved Quantities

An obvious question to ask is whether our discrete Maxwell's equations have conserved quantities analogous to those for the continuum equations. The simplest to start with is the conservation of charge. If we consider the quantity,

$$\nabla_q^- \cdot \hat{\varepsilon}(\mathbf{r}) \hat{\mathbf{E}}(\mathbf{r}) \quad (30)$$

And then calculate the discrete version of its time derivative,

$$\begin{aligned}
\Delta_{\tau}^{-} \cdot \nabla_q^{-} \cdot \hat{\varepsilon}(\mathbf{r}) \hat{\mathbf{E}}(\mathbf{r}) &= \nabla_q^{-} \cdot \Delta_{\tau}^{-} \cdot \hat{\varepsilon}(\mathbf{r}) \hat{\mathbf{E}}(\mathbf{r}) \\
&= \nabla_q^{-} \cdot \nabla_q^{-} \times \hat{\mathbf{H}}' \\
&= 0
\end{aligned} \tag{31}$$

Because our approximations to Maxwell's equations have preserved the form of the curls, the quantity $\nabla_q^{-} \cdot \hat{\varepsilon}(\mathbf{r}) \hat{\mathbf{E}}(\mathbf{r})$ remains an exactly conserved quantity even on the discrete lattice. This is the direct equivalent of $\nabla \cdot \mathbf{D}$ being conserved in the continuum case, in other words, of the conservation of charge. The same follows for $\nabla_q^{+} \cdot \hat{\mu}(\mathbf{r}) \hat{\mathbf{H}}'(\mathbf{r})$ corresponding to the conservation of the 'magnetic charge', $\nabla \cdot \mathbf{B}$.

The next task is to find the correct form for Poynting's theorem on the lattice. This again follows in a straightforward way in our formalism if we begin from the following form for the energy density.

$$U(t) = \frac{1}{2} [\varepsilon_0 \varepsilon(\mathbf{r}) E_{\alpha}^*(\mathbf{r}, t) E^{\alpha}(\mathbf{r}, t - \delta t) + \mu_0 \mu(\mathbf{r}) H_{\alpha}^*(\mathbf{r}, t - \delta t) H^{\alpha}(\mathbf{r}, t - \delta t)] \tag{32}$$

This has the correct form for the energy density in the limit $\delta t \rightarrow 0$. Substituting the expressions for the generalised co-ordinates we obtain,

$$U(t) = \frac{U_0}{2} \left[\hat{\varepsilon}^{\alpha\beta} \hat{E}_{\alpha}^*(\mathbf{r}, t) \hat{E}_{\beta}(\mathbf{r}, t - \delta t) + \left(\frac{Q_0}{c_0 \delta t} \right)^2 \hat{\mu}^{\alpha\beta} \hat{H}'_{\alpha}(\mathbf{r}, t - \delta t) \hat{H}'_{\beta}(\mathbf{r}, t - \delta t) \right] \tag{33}$$

where $U_0 = Q_0 \varepsilon_0 / (Q_1 Q_2 Q_3 |\mathbf{u}_1 \cdot \mathbf{u}_2 \times \mathbf{u}_3|)$. Poynting's theorem can then be obtained by considering the time difference operator $\Delta_t U(t) = (U(t + \delta t) - U(t)) / \delta t$. This gives,

$$\begin{aligned}
\Delta_t^+ U(t) &= \frac{U_0}{2} \left\{ \left[\hat{H}'_2(\mathbf{r} - \mathbf{c}, t) - \hat{H}'_3(\mathbf{r} - \mathbf{b}, t) \right] \hat{E}_1(\mathbf{r}, t) \right. \\
&\quad + \left[\hat{H}'_3(\mathbf{r} - \mathbf{a}, t) - \hat{H}'_1(\mathbf{r} - \mathbf{c}, t) \right] \hat{E}_2(\mathbf{r}, t) \\
&\quad + \left[\hat{H}'_1(\mathbf{r} - \mathbf{b}, t) - \hat{H}'_2(\mathbf{r} - \mathbf{a}, t) \right] \hat{E}_3(\mathbf{r}, t) \\
&\quad + \left[\hat{H}'_2(\mathbf{r} - \mathbf{c}, t - \delta t) - \hat{H}'_3(\mathbf{r} - \mathbf{b}, t - \delta t) \right] \hat{E}_1^*(\mathbf{r}, t) \\
&\quad + \left[\hat{H}'_3(\mathbf{r} - \mathbf{a}, t - \delta t) - \hat{H}'_1(\mathbf{r} - \mathbf{c}, t - \delta t) \right] \hat{E}_2^*(\mathbf{r}, t) \\
&\quad + \left[\hat{H}'_1(\mathbf{r} - \mathbf{b}, t - \delta t) - \hat{H}'_2(\mathbf{r} - \mathbf{a}, t - \delta t) \right] \hat{E}_3^*(\mathbf{r}, t) \\
&\quad + \left[\hat{E}_2(\mathbf{r} + \mathbf{c}, t) - \hat{E}_3(\mathbf{r} + \mathbf{b}, t) \right] \hat{H}'_1(\mathbf{r}, t) \\
&\quad + \left[\hat{E}_3(\mathbf{r} + \mathbf{a}, t) - \hat{E}_1(\mathbf{r} + \mathbf{c}, t) \right] \hat{H}'_2(\mathbf{r}, t) \\
&\quad + \left[\hat{E}_1(\mathbf{r} + \mathbf{b}, t) - \hat{E}_2(\mathbf{r} + \mathbf{a}, t) \right] \hat{H}'_3(\mathbf{r}, t) \\
&\quad + \left[\hat{E}_2^*(\mathbf{r} + \mathbf{c}, t) - \hat{E}_3^*(\mathbf{r} + \mathbf{b}, t) \right] \hat{H}'_1(\mathbf{r}, t) \\
&\quad + \left[\hat{E}_3^*(\mathbf{r} + \mathbf{a}, t) - \hat{E}_1^*(\mathbf{r} + \mathbf{c}, t) \right] \hat{H}'_2(\mathbf{r}, t) \\
&\quad + \left. \left[\hat{E}_1^*(\mathbf{r} + \mathbf{b}, t) - \hat{E}_2^*(\mathbf{r} + \mathbf{a}, t) \right] \hat{H}'_3(\mathbf{r}, t) \right\} \tag{34}
\end{aligned}$$

The important point to notice is that when this quantity is summed over a set of neighbouring lattice points only the terms associated with the surface of the integration region survive, all the volume terms cancel. This allows us to identify the right hand side of equation (34) as the Poynting vector integrated over the volume surrounding one lattice point.

III. OBTAINING THE GREEN'S FUNCTION ON THE LATTICE

We turn our attention now to consider how we can define the Green's function within our discrete real space formalism. We will begin from the continuum limit, and write Maxwell's equations as

$$\mathbf{M} \begin{pmatrix} \mathbf{E} \\ \mathbf{H} \end{pmatrix} = \omega \mathbf{P} \begin{pmatrix} \mathbf{E} \\ \mathbf{H} \end{pmatrix} \tag{35}$$

where,

$$\mathbf{M} = \begin{pmatrix} 0 & +i\nabla \times \\ -i\nabla \times & 0 \end{pmatrix} \quad ; \quad \mathbf{P} = \begin{pmatrix} \varepsilon(\mathbf{r})\varepsilon_0 & 0 \\ 0 & \mu(\mathbf{r})\mu_0 \end{pmatrix} \quad (36)$$

We now define a six vector,

$$\mathbf{F}_s = \begin{pmatrix} \mathbf{E}_s \\ \mathbf{H}_s \end{pmatrix} \quad (37)$$

as an eigenfunction of equation 35 with an eigenvalue ω_s . We choose to normalise the \mathbf{F} 's such,

$$\int \sum_{j=1}^6 \sum_{j'=1}^6 F_{s,j}^\dagger(\mathbf{r}) P_{jj'} F_{s',j'}(\mathbf{r}) d^3\mathbf{r} = \delta_{ss'} \quad (38)$$

And the completeness relation gives us,

$$\sum_{s,j''} F_{s,j}(\mathbf{r}) F_{s,j''}^\dagger(\mathbf{r}') P_{jj''} = \delta_{jj'} \delta(\mathbf{r} - \mathbf{r}') \quad (39)$$

We can define a Green's function in the usual way,

$$G_{jj'}^R(\omega, \mathbf{r}, \mathbf{r}') = \sum_{s,j''} \frac{F_j(s, \mathbf{r}) F_{j''}^\dagger(s, \mathbf{r}') P_{j''j'}}{\omega - \omega_s + i\delta} \quad (40)$$

The Green's function clearly obeys the equation,

$$(\omega - \mathbf{P}^{-1}\mathbf{M})G_{ij}^R(\omega, \mathbf{r}, \mathbf{r}') = \delta_{ij} \delta(\mathbf{r} - \mathbf{r}') \quad (41)$$

We can now Fourier transform to obtain the Green's function in the time domain,

$$\begin{aligned} G_{jj'}^R(t, \mathbf{r}, \mathbf{r}') &= \frac{1}{2\pi} \int_{-\infty}^{+\infty} G_{jj'}^R(\omega, \mathbf{r}, \mathbf{r}') e^{-i\omega t} d\omega \\ &= -i \sum_{s,j''} F_{s,j}(\mathbf{r}) F_{s,j''}^\dagger(\mathbf{r}') P_{j''j'} e^{-i\omega_s t} \end{aligned} \quad (42)$$

so that,

$$\left(i \frac{\partial}{\partial t} - \mathbf{P}^{-1}\mathbf{M} \right) \mathbf{G}^R(t, \mathbf{r}, \mathbf{r}') = \delta(t) \delta(\mathbf{r} - \mathbf{r}') \quad (43)$$

Now we turn to consider how to repeat this procedure for the discrete case. We begin from equation 35, but apply the substitutions for \mathbf{k}, ω presented in the previous section,

$$\mathbf{P}^{-1}\mathbf{M} \begin{pmatrix} \mathbf{E}(\mathbf{r}, t) \\ \mathbf{H}(\mathbf{r}, t) \end{pmatrix} = i \begin{pmatrix} \Delta_t^+ & 0 \\ 0 & \Delta_t^- \end{pmatrix} \begin{pmatrix} \mathbf{E}(\mathbf{r}, t) \\ \mathbf{H}(\mathbf{r}, t) \end{pmatrix} \quad (44)$$

where \mathbf{M} is now

$$\mathbf{M} = \begin{pmatrix} 0 & +i\nabla^- \times \\ -i\nabla^- \times & 0 \end{pmatrix} \quad (45)$$

We want to construct the $\mathbf{G}^R(t)$ which will obey the equation

$$\left[i \begin{pmatrix} \Delta_t^+ & 0 \\ 0 & \Delta_t^- \end{pmatrix} - \mathbf{P}^{-1}\mathbf{M} \right] \mathbf{G}^R(t, \mathbf{r}, \mathbf{r}') = \delta(t) \delta(\mathbf{r} - \mathbf{r}') \quad (46)$$

Try constructing,

$$\begin{aligned}
G_{jj'}^R(t, \mathbf{r}, \mathbf{r}') &= -i\delta t \sum_{s,j''} F_{s,j}(\mathbf{r}) F_{s,j''}^\dagger(\mathbf{r}') P_{j''j'} e^{-i\omega_s(t-\delta t)}; t > 0 \\
G_{jj'}^R(t, \mathbf{r}, \mathbf{r}') &= 0 \quad ; t \leq 0
\end{aligned} \tag{47}$$

then,

$$\begin{aligned}
G_{jj'}^R(\omega, \mathbf{r}, \mathbf{r}') &= \sum_{t=\delta t}^{N_t \delta t} G_{jj'}^R(t, \mathbf{r}, \mathbf{r}') e^{i\omega t} \\
&= -i\delta t \sum_{s,j''} F_{s,j}(\mathbf{r}) F_{s,j''}^\dagger(\mathbf{r}') P_{j''j'} \left[\frac{1 - e^{i(\omega - \omega_s)N_t \delta t}}{e^{-i(\omega - \omega_s)\delta t} - 1} \right] e^{i\omega_s \delta t}
\end{aligned} \tag{48}$$

If N_t is large and $\omega = \omega + i\delta$,

$$G_{jj'}^R(\omega, \mathbf{r}, \mathbf{r}') = -i\delta t \sum_{s,j''} F_{s,j}(\mathbf{r}) F_{s,j''}^\dagger(\mathbf{r}') P_{j''j'} \frac{e^{i\omega_s \delta t}}{e^{-i(\omega - \omega_s)\delta t} - 1} \tag{49}$$

which in the limit $\delta t \rightarrow 0$ gives the correct form for the frequency dependent Green's function. So simply by setting $t = \delta t$ in equation 47 to give,

$$G_{jj'}^R(t = \delta t, \mathbf{r}, \mathbf{r}') = -i \delta t \delta_{jj'} \delta(\mathbf{r} - \mathbf{r}') \tag{50}$$

as the appropriate starting condition and applying equation (44) we can calculate $\mathbf{G}^R(t)$ at all subsequent times.

Once we have found the Green's function it is a simple matter to calculate useful physical quantities from it, such as the photonic density of states. The local density of states, for example, is found in the usual way, from the imaginary part of the trace of $G^R(\omega)$ ¹⁵.

$$\rho(\omega, \mathbf{r}) = -\frac{1}{\pi} \text{Im} \left[\sum_j G_{jj}^R(\omega, \mathbf{r}, \mathbf{r}) \right] \tag{51}$$

Similarly, the band structure can be easily determined by locating the poles in the Green's function and so identifying the normal modes of the system.

IV. RESULTS

We shall now put the ideas of the previous sections to work for two different physical systems.

A. Bragg Stack

In the first case we will look at what is probably the simplest one dimensional photonic crystal that can be imagined, the dielectric multilayer, or Bragg stack. This crystal is formed by stacking together alternating layers of dielectric of high and low refractive index (see figure 1). Each layer is of infinite extent in the plane and we choose parameters such that the high refractive index ($n = 3.6$) planes have a thickness of $0.3a$ and the low index ($n = 1.0$) planes have a thickness of $0.7a$ where a is the lattice spacing. This choice leads to a sizable band gaps for electromagnetic waves propagating normal to the planes as can be seen in figure 2. The frequencies in this figure are scaled so as to be dimensionless, what we actually write for the frequency is $\omega a / (2\pi c_0)$. The wavevectors are also written in dimensionless units of $k.a$ so that the edge of the first Brillouin zone occurs at $\pm\pi$.

In figure 3 we show the local density of states for a point inside the Bragg stack. Again the frequencies are given in dimensionless units and the density of states itself is in arbitrary units. The band gaps are clearly visible as frequency windows over which the density of states is strongly suppressed. At the band edges the Van Hove singularities are also apparent corresponding to the points on the band structure at the band edges where $\partial\omega/\partial k$ tends to zero.

We can go one step further and add a defect layer to the otherwise perfect crystal. We do this by introducing a supercell consisting of 25 repeat units of the Bragg stack, then a defect of $0.3a$ of the high refractive index material, and then another 25 unit cells. The local density of states at the centre of the defect can be seen in figure 4 superimposed over the density of states for the perfect crystal. The dominant feature are the new peaks which have appeared in the band gaps. These correspond to localised modes associated with the defect. That these modes are tightly localised can be easily shown by calculating the local density of states in the crystal several lattice spacings away from the defect. The perfect crystal result is recovered.

B. Diamond Lattice

The second system which we shall consider is a fully three dimensional photonic crystal made up from air spheres embedded in a dielectric host arranged in a diamond lattice structure. This structure was one of the first to be shown to have a complete photonic band gap⁹. Figure 5 gives a diagram of the diamond structure and indicates the unit cell which we choose. This unit cell is not primitive but is chosen for convenience with lattice vectors; $\mathbf{a} = a\mathbf{i}$, $\mathbf{b} = (a/2)\mathbf{i} + (\sqrt{3}a/2)\mathbf{j}$ and $\mathbf{c} = \sqrt{6}ak$ where a is the distance between nearest neighbour lattice points. The exact parameters we have chosen lead to a fairly sizable band gap. The refractive index for the host material is $n = 3.6$, the spheres have $n = 1.0$, and the ratio of sphere radius to the distance separating nearest neighbour spheres is 0.43. The band structure for this system in the directions $\Gamma - K$ and $\Gamma - X$ is given in figure 6 where it is clear that a band gap is opening up over a frequency range of about 3.2 and 3.9 in dimensionless units. This band gap is confirmed in the density of states, in figure 7. The density of states calculation is performed by creating a super-cell by stacking unit cells together, eight in each direction. Because each of our unit cells is not in fact primitive but itself contains three primitive cells, the super-cell consists of 1536 primitive units cells. By creating a larger unit cell we reduce the number of \mathbf{k} -points which we need to sample in order to build up the complete local density of states.

Next we can introduce a defect into the diamond lattice by again creating a super-cell by stacking unit cells together and then cutting a hole in one of the dielectric parts of the cell. This defect will have a localised defect mode associated with it and by altering the amount of dielectric material we cut away we can tune the frequency of the mode. We choose the size of the defect so that the defect mode lies within the band gap for the crystal. We cut away a parallelepiped region spanning adjacent unit cells starting from $(\mathbf{a}/2, \mathbf{b}/3, \mathbf{c}/3)$ and with edges of $5\mathbf{a}/6$, $5\mathbf{b}/6$ and $5\mathbf{c}/12$. Figure 8 shows the density of states for the super-cell with the defect and as for the Bragg stack case, several defect modes are clearly seen. We have also checked that we have made the super-cell sufficiently large by testing that the position of the defect mode peaks do not disperse with \mathbf{k} .

V. CONCLUSIONS

In this paper we have shown how an Order-N, finite difference time domain method can be used to calculate the Green's function in a simple and straightforward way. Specifically, our new formalism enables us to give a simple derivation for the numerical stability criterion, exact statements of charge and energy conservation and allows us to use non-orthogonal co-ordinate systems without the usual computational overheads.

From the Green's function a whole range of other physical quantities can be found such as the local density of states. The times required to calculate these quantities scales linearly with the size of the system, so our technique is of particular importance in analysing systems with very large or complicated unit cells. Specifically, we have calculated the local density of states for both a one and three dimensional photonic crystal containing a defect and have recovered the expected result. The defect has the effect of introducing a highly localised mode the frequency of which is determined by the size of the defect. By a careful choice we have found defect states within the photonic band gap for the crystal. These localised states have potential application in photonic cavity laser structures where the efficiency of the laser is enhanced by suppression of emission into all but the lasing mode. The linear scaling of this method with system size should allow modelling of realistic designs for cavity structures without prohibitive computational overheads associated with traditional computational schemes.

The computer program used to calculate the results presented in this paper has recently been submitted to the CPC International Program Library¹⁶.

¹ K. S. Yee, IEEE Trans. Antennas Propag. **14**, 302 (1966).

² C. T. Chan, Q. L. Yu, and K. M. Ho, Phys. Rev. B **51**, 16635 (1995).

³ J. B. Pendry, J. Phys.: Condens. Matter **8**, 1085 (1996).

⁴ E. Yablonovitch, J. Phys.: Condens. Matter **5**, 2443 (1993).

⁵ E. Yablonovitch and T. J. Gmitter, Phys. Rev. Lett. **63**, 1950 (1989).

⁶ H. Hirayama, T. Hamano, and Y. Aoyagi, RIKEN Super Computing Prog. Rep. **1**, 1 (1996).

⁷ K. M. Leung and Y. F. Liu, Phys. Rev. Lett. **65**, 2646 (1990).

⁸ Z. Zhang and S. Satpathy, Phys. Rev. Lett. **65**, 2650 (1990).

⁹ K. M. Ho, C. T. Chan, and C. M. Soukoulis, Phys. Rev. Lett. **65**, 3152 (1990).

¹⁰ J. B. Pendry and A. MacKinnon, Phys. Rev. Lett. **69**, 2772 (1992).

¹¹ J. B. Pendry, J. Mod. Optics **41**, 209 (1994).

¹² F. Wijnands *et al.*, Optical and Quantum Electronics **29**, 199 (1997).

¹³ J. Lee, R. Palandech, and R. Mittra, IEEE Trans. Microwave Theory Tech. **40**, 346 (1992).

¹⁴ A. J. Ward and J. B. Pendry, J. Mod. Optics **43**, 773 (1995).

¹⁵ E. N. Economou, *Green's Functions in Quantum Physics* (Springer-Verlag, Berlin, 1990).

¹⁶ A. J. Ward and J. B. Pendry, A Program for Calculating Photonic Band Structures and Green's Functions using a non-orthogonal FDTD Method, Submitted to Computer Physics Commun.

FIG. 1. A dielectric multilayer or Bragg stack formed by alternating layers of high (shaded) and low (unshaded) permittivity materials. The thickness of the high dielectric layer is d and the lattice period is a

FIG. 2. The photonic band structure for Bragg stack

FIG. 3. The density of states for the ideal Bragg stack. The Van Hove singularities in the perfect crystal are clearly seen

FIG. 4. The density of states both with and without a defect inserted into the ideal Bragg stack. Both the Van Hove singularities in the perfect crystal and the localised state associated with the defect are clearly seen

FIG. 5. Diagram of the diamond lattice. The bravais lattice is FCC and the lattice points are shown as the black dots. On each lattice point are placed two 'atoms' - dielectric spheres in our case; one at $(0, 0, 0)$, one at $(0, 0, c/4)$, where $c = \sqrt{6}a$. Some of the 'atoms' are shown as the grey circles. The unit cell we model is the parallelepiped enclosed by the thick black lines

FIG. 6. Partial band structure for spheres on the diamond lattice in the $\Gamma - K$ and $\Gamma - X$ directions. The presence of the band gap is clearly shown

FIG. 7. The density of states for the diamond structure

FIG. 8. The density of states both with and without a defect for the diamond structure. The localised state associated with the defect is clearly seen

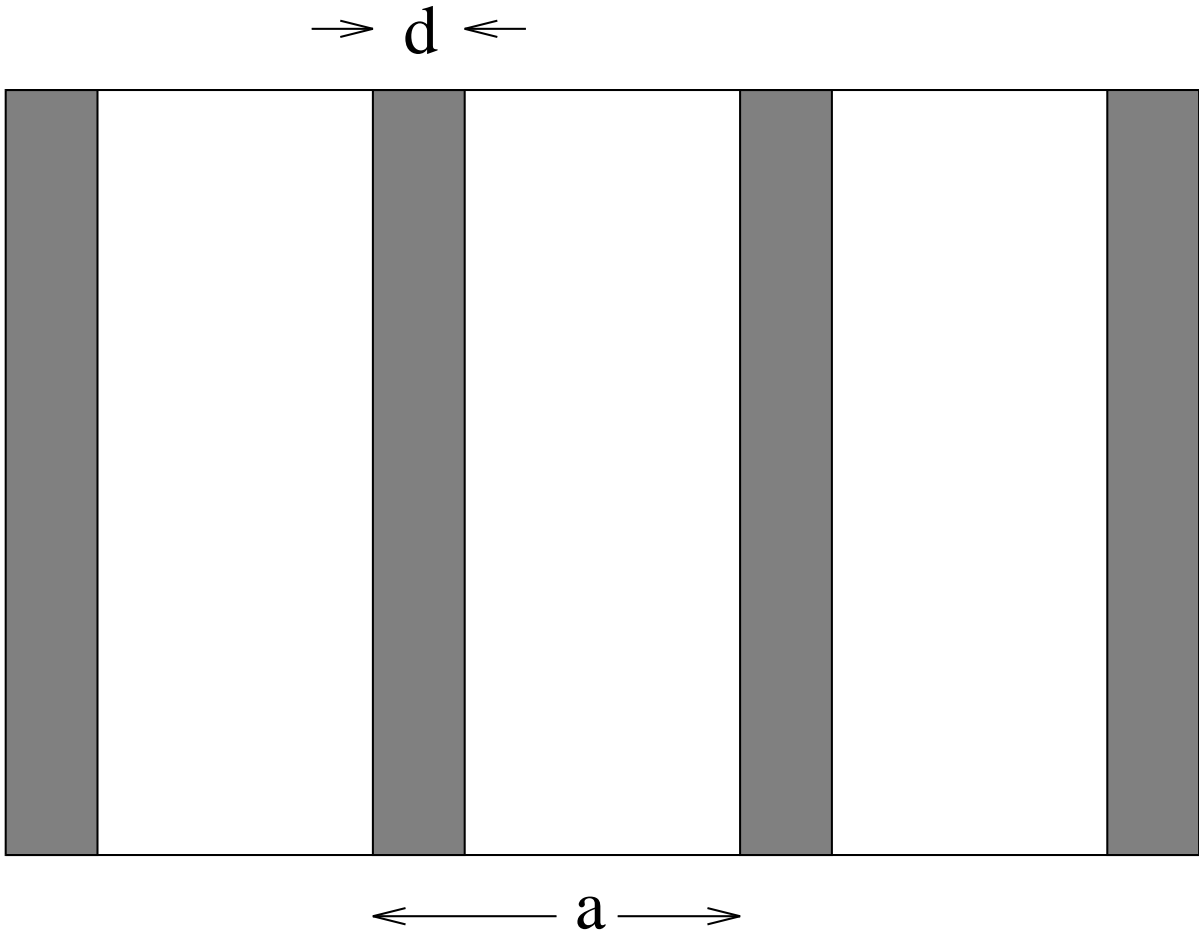


Figure 1

A. J. Ward, J. B. Pendry

Calculating photonic Green's functions using a non-orthogonal,
finite difference time domain method

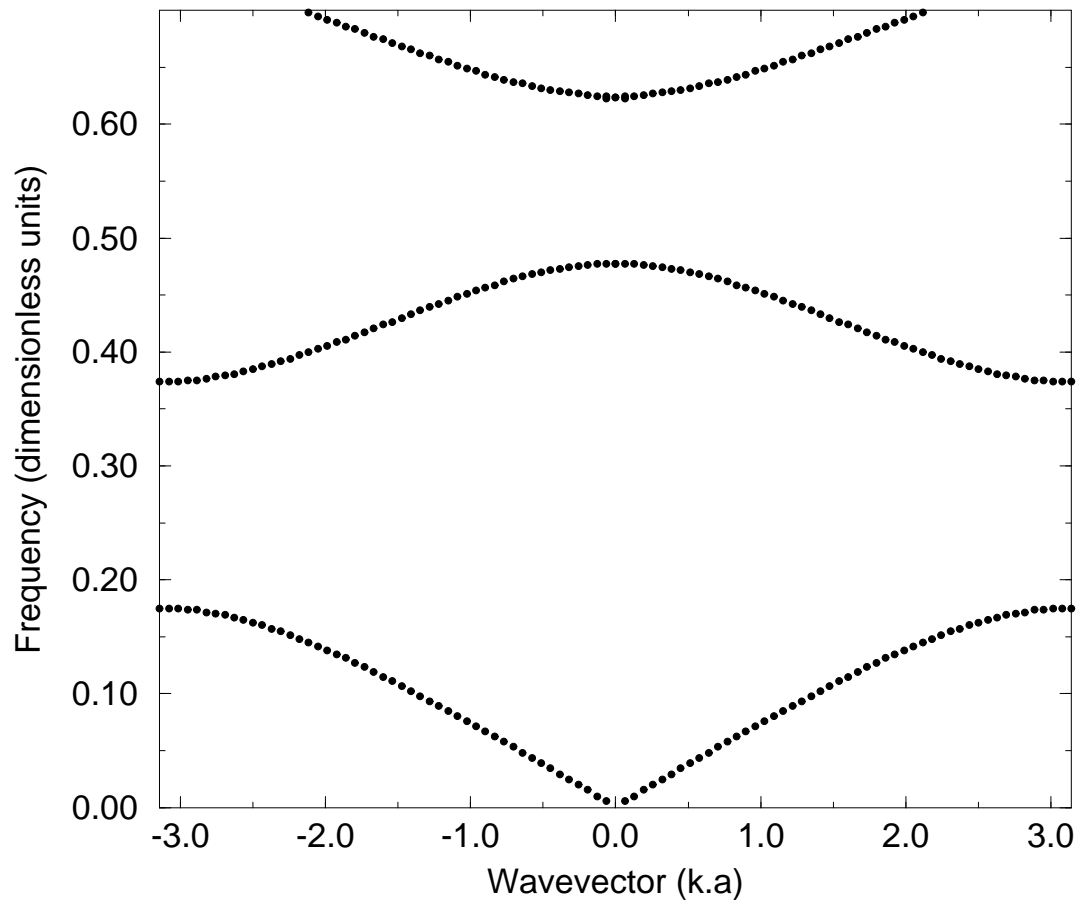


Figure 2

A. J. Ward, J. B. Pendry

Calculating photonic Green's functions using a non-orthogonal,
finite difference time domain method

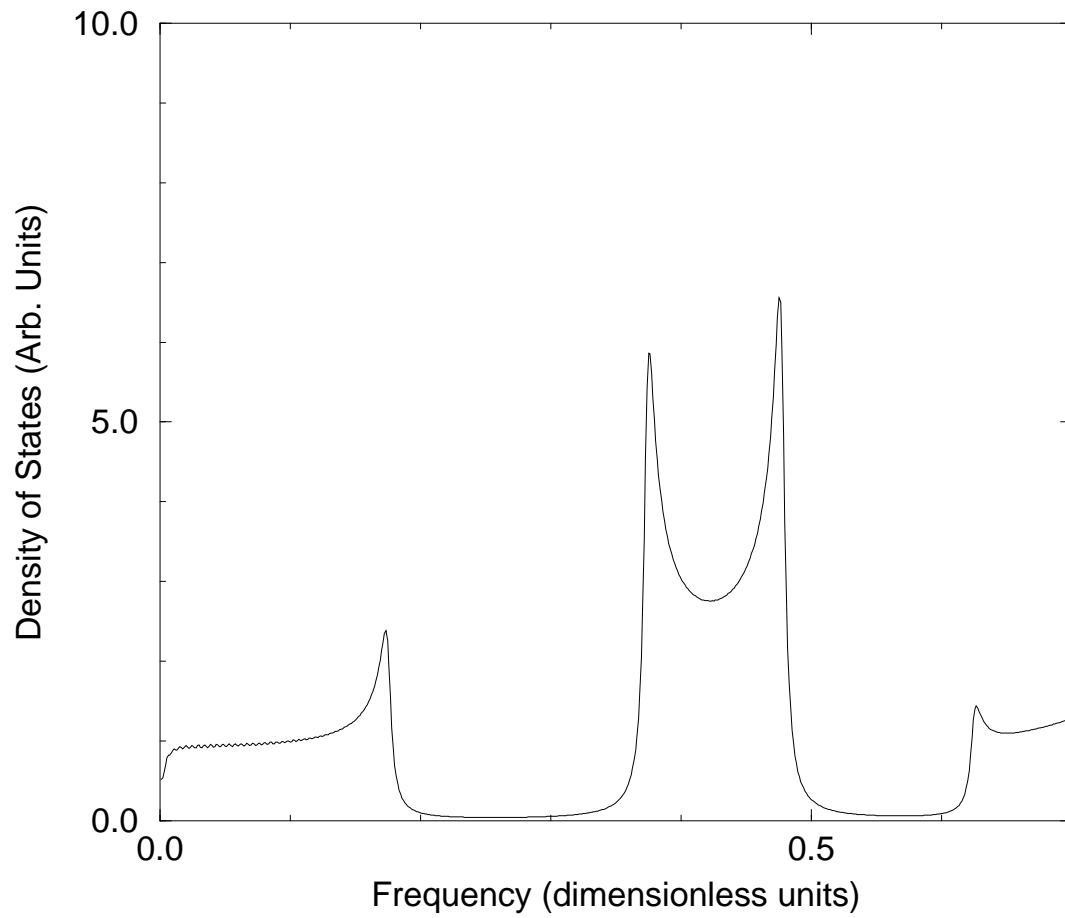


Figure 3

A. J. Ward, J. B. Pendry

Calculating photonic Green's functions using a non-orthogonal,
finite difference time domain method

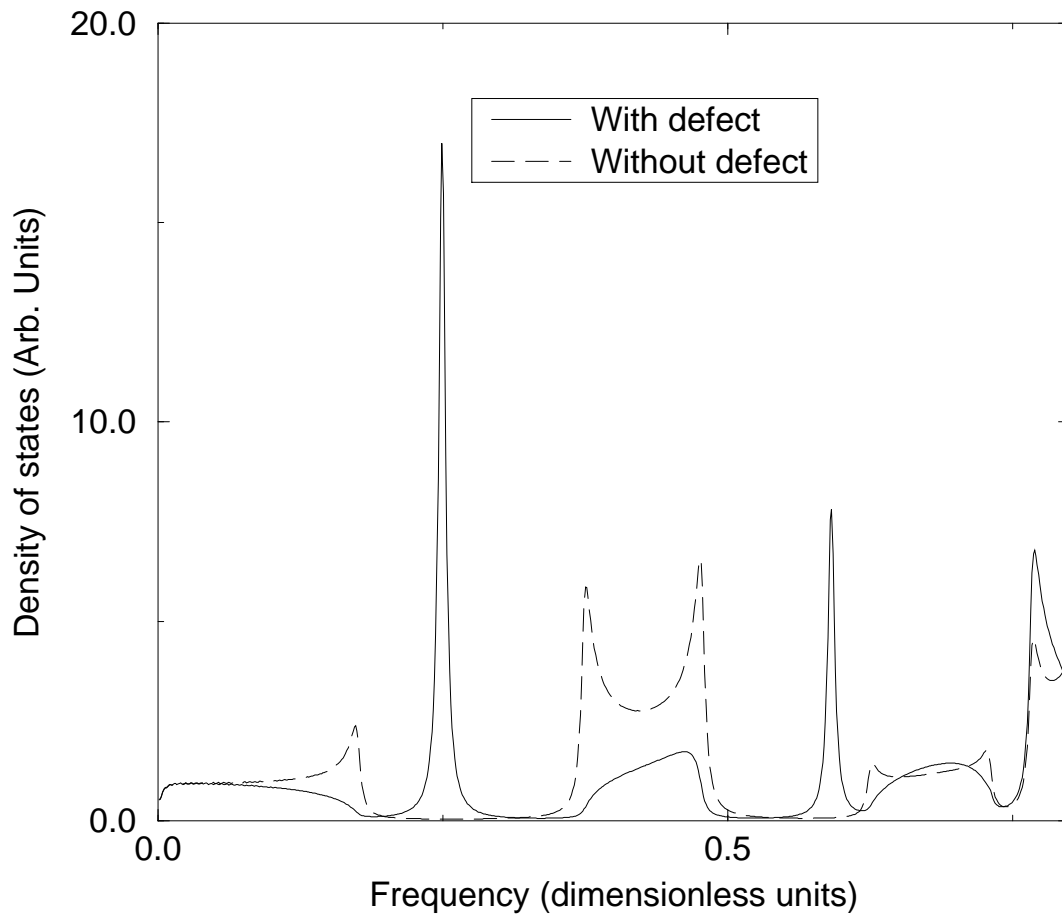


Figure 4

A. J. Ward, J. B. Pendry

Calculating photonic Green's functions using a non-orthogonal,
finite difference time domain method

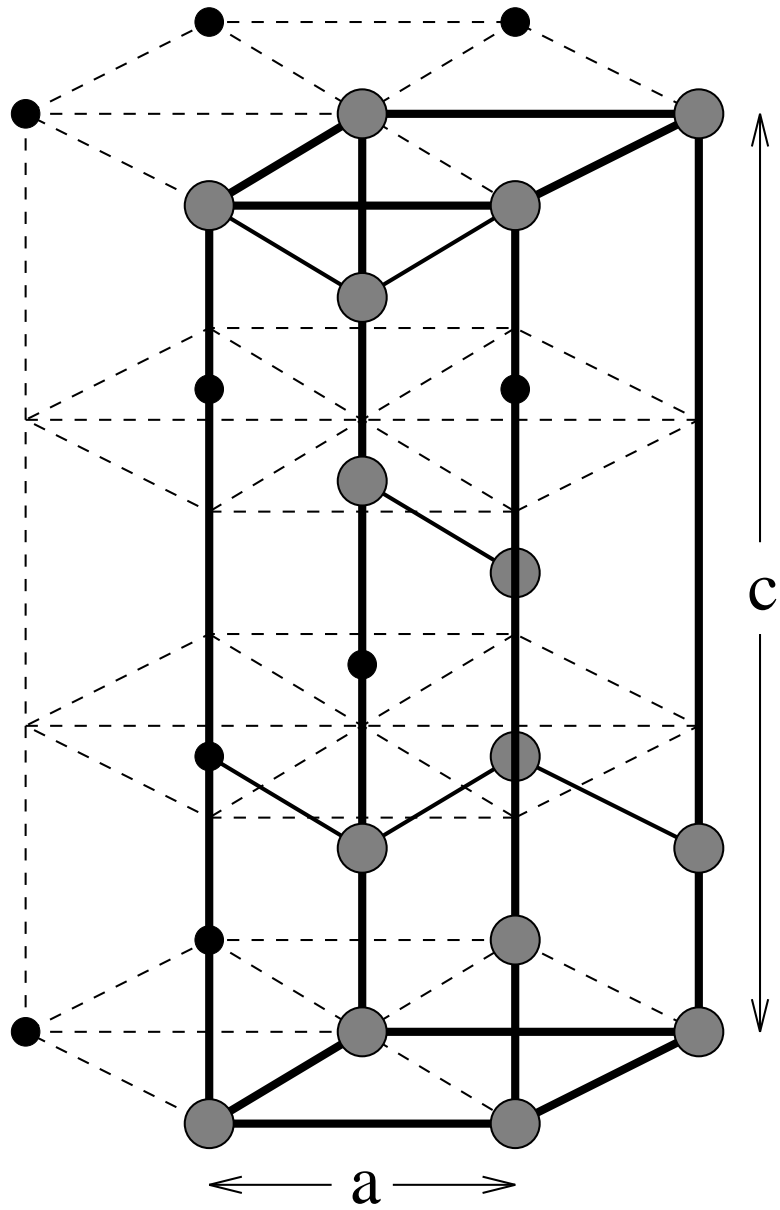


Figure 5

A. J. Ward, J. B. Pendry

Calculating photonic Green's functions using a non-orthogonal,
finite difference time domain method

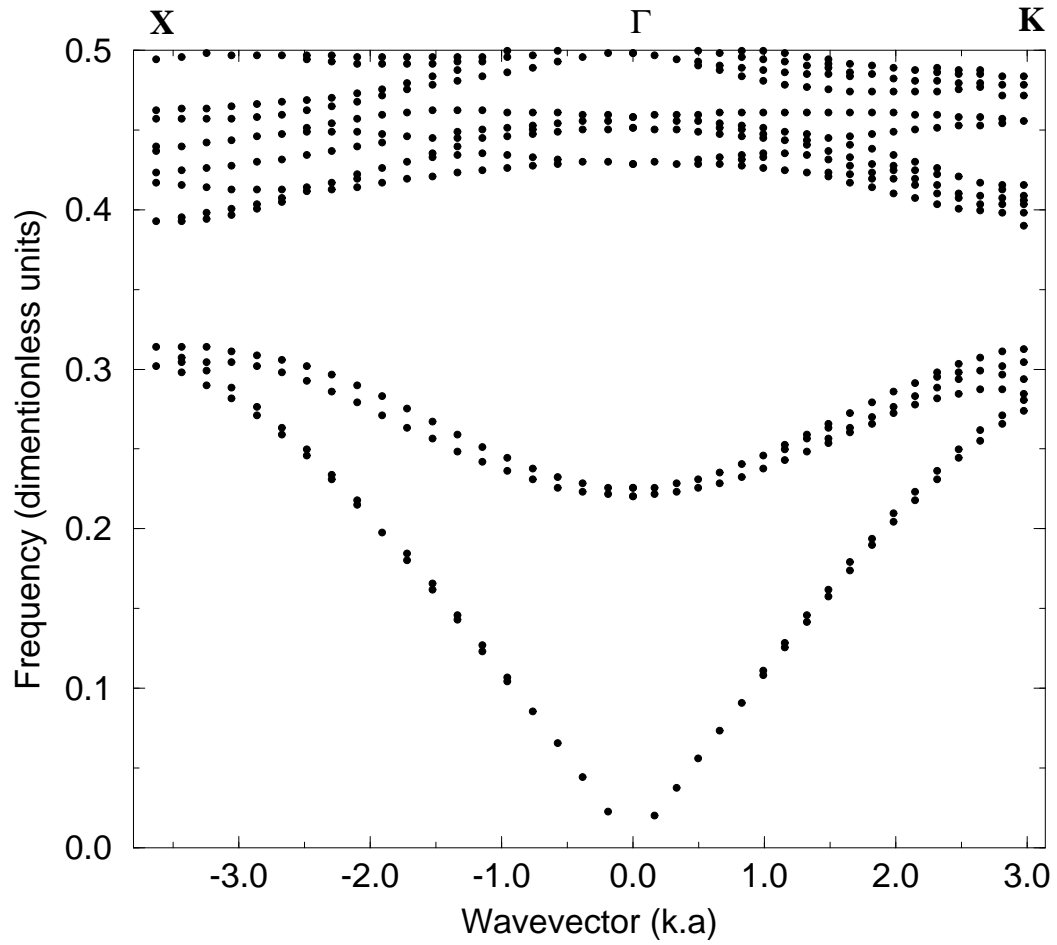


Figure 6

A. J. Ward, J. B. Pendry

Calculating photonic Green's functions using a non-orthogonal,
finite difference time domain method

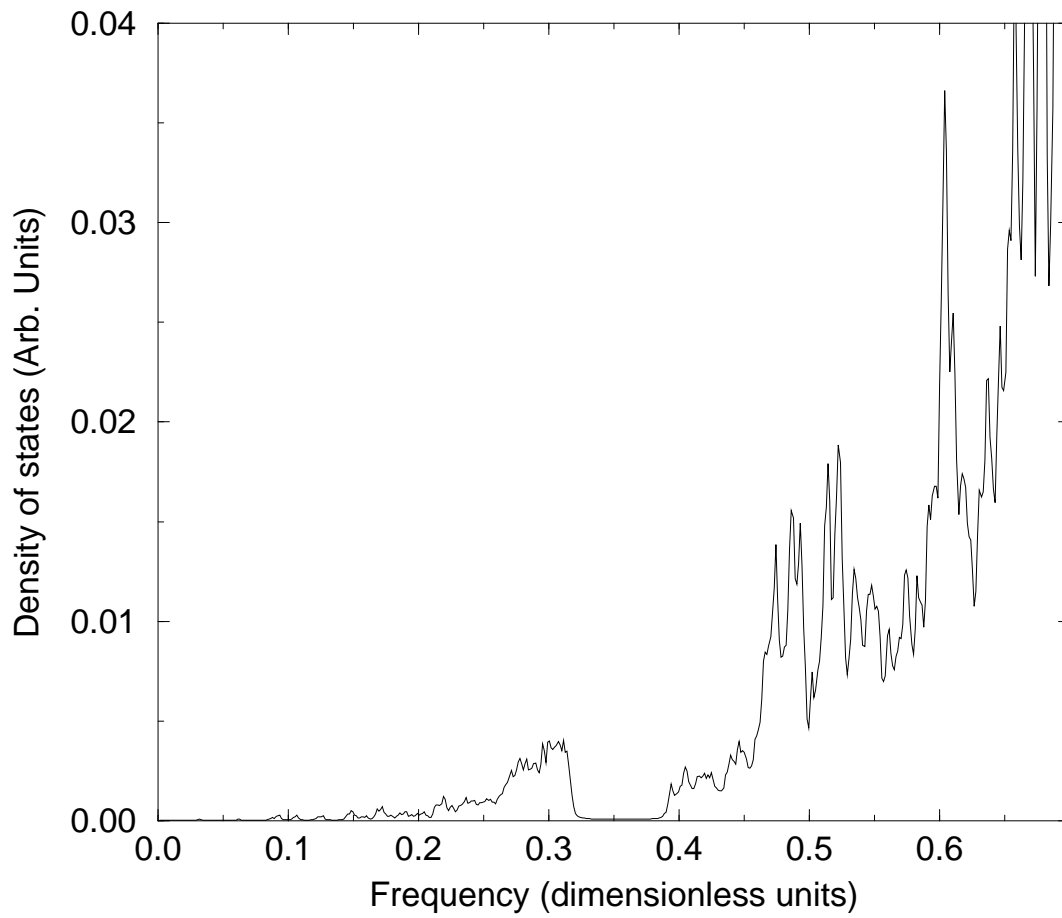


Figure 7

A. J. Ward, J. B. Pendry

Calculating photonic Green's functions using a non-orthogonal,
finite difference time domain method

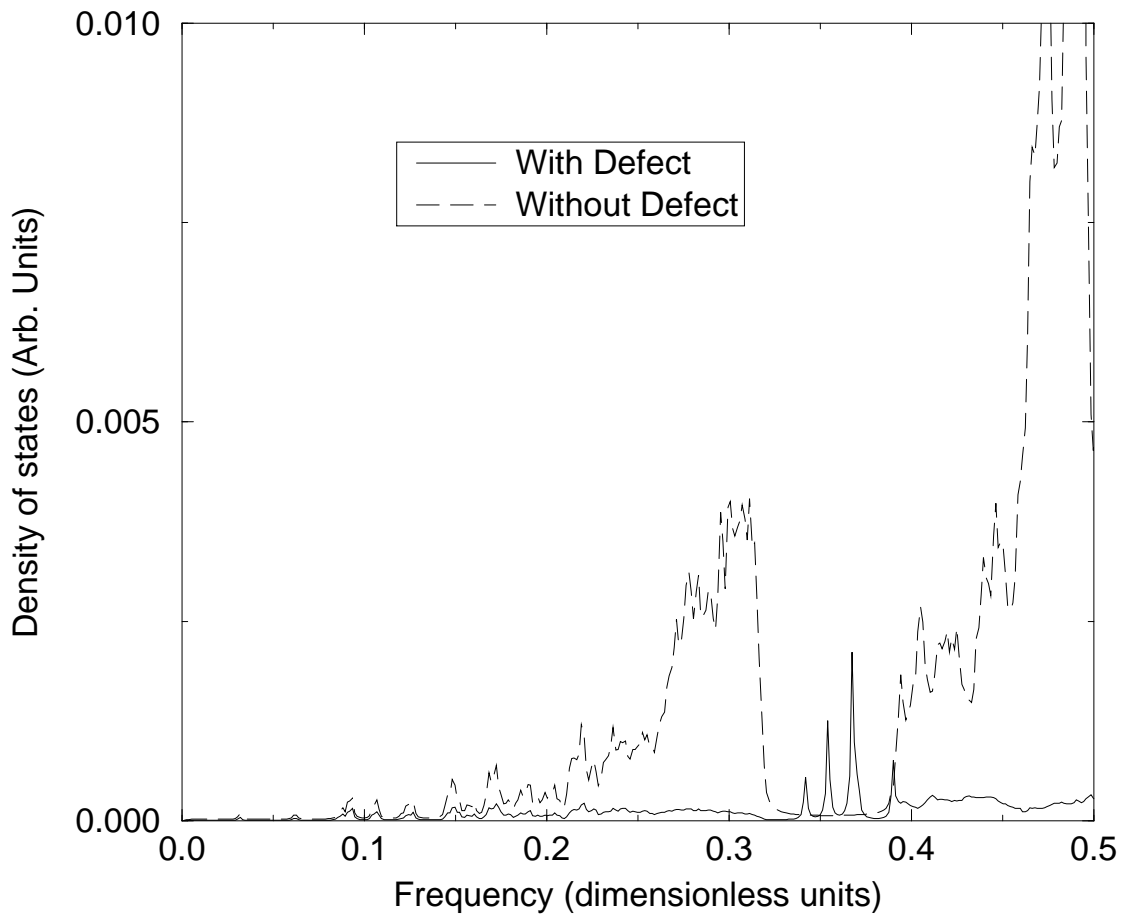


Figure 8

A. J. Ward, J. B. Pendry

Calculating photonic Green's functions using a non-orthogonal,
finite difference time domain method